Photodegradable Hydrogels for On-Demand Modeling of Age-Related Spatiotemporal ECM Deformation

Felix Reul[1,2], Cédric Bergerbit[2,3,4], Iulia Scarlat[1,2], Teodora Piskova[1,2], Vasudha Turuvekere Krishnamurthy[1,2], Aleksandra Kozyrina[1,2], Stacy Lok Sze Yam[1,2], Laura De Laporte[2,3,4] and Jacopo Di Russo[1,2]

[1]Institute of Molecular and Cellular Anatomy, RWTH Aachen University, Germany
[2]DWI-Leibniz-Institute for Interactive Materials, Aachen, Germany
[3]Department of Advanced Materials for Biomedicine (AMB), CBMS—Center for Biohybrid Medical Systems, AME—Institute of Applied Medical Engineering, RWTH Aachen University, Germany
[4]Institute for Technical and Macromolecular Chemistry, Chair for Macromolecular Materials for Medicine RWTH Aachen University, Germany

Key words: Photodegradable Hydrogel; ECM; Topography; Epithelium; RPE; Aging

Correspondence:

Jacopo Di Russo

jdirusso@ukaachen.de

Abstract

The extracellular matrix (ECM) plays a crucial role in regulating tissue behavior through a dynamic interplay of spatial and temporal cues. Dynamic materials capable of modulating these cues at relevant scales are essential for tackling current challenges in tissue engineering and addressing fundamental biological questions. In vision research, there is a notable lack of suitable *in vitro* systems to study ECM dynamics. To help fill this gap, we developed an easy-to-use, photosensitive poly(ethylene glycol)-based hydrogel that can deform on demand to simulate ECM bulging, known as drusen, associated with the aging of the outer retina. Our findings demonstrate that variations in the size of these artificial drusen during culture impact morphometric parameters of the retinal pigment epithelium, offering new insights into its mechanical resilience to different drusen sizes. Notably, drusen formation in our system does not significantly affect the cellular actin cytoskeleton or polarity, which are often disrupted in conventional acute substrate deformation models. In summary, we present a light-tunable hydrogel platform that enables precise spatial and temporal mimicry of ECM topographical changes, offering a promising tool for investigating the mechanobiological aspects of dynamic cell-matrix interactions.

Introduction

The extracellular matrix (ECM) is a fundamental, non-cellular component of all tissues and organs. Beyond providing the structural scaffolding that sustains tissue architecture, it acts as a dynamic regulator of cellular behavior in tissues [1–3]. Tissues continuously evolve through morphogenesis, homeostasis, and aging, with the ECM providing a dynamic array of biochemical, topological, and physical cues [1–3]. Mimicking these dynamic changes at a relevant time and length scale in a laboratory setting is therefore crucial for overcoming current challenges in tissue engineering and addressing basic biological questions. This is evident in advanced stem cell-derived tissues, which closely replicate the metabolic activity, tissue architecture, and developmental timing found *in vivo*. Unlike conventional, fast-proliferating immortalized cell lines, stem cell-derived systems grow and differentiate in a more controlled and coordinated manner, mirroring the slower pace and complex spatial organization of native tissues[4,5]. As a result, recreating the dynamic interplay between cells and the ECM over realistic timescales is essential to fully harness the potential of stem cell-derived models for studying fundamental processes, such as tissue remodeling, disease progression, and aging under near-physiological conditions[4].

Vision research faces major challenges due to the lack of relevant *in vitro* model systems, as animal models often fail to accurately replicate the anatomy, physiology, and disease mechanisms of the human eye. In particular, modeling key age-related changes in the ECM seen in humans remains challenging in animal systems, creating a significant barrier to a comprehensive understanding of the pathophysiology of eye diseases[6,7]. One significant age-related change in the ECM of the eye is the local accumulation of lipids and proteins underneath the retinal pigment epithelium (RPE), named drusen. The morphology and composition of drusen differ among individuals. However, epidemiological studies have indicated that medium (63 – 125 µm in diameter) and large (> 125 µm in diameter) drusen, with a height of 17-30 µm, are associated with phenotypical changes and polarity loss in RPE cells. This progression ultimately leads to photoreceptor degeneration and contributes to the development of age-related macular degeneration or AMD [8,9]. In the past, diverse approaches have been employed to mimic drusen formation and study the consequences on RPE *in vitro*. Here, techniques such as vacuum, magnetic, piston, or air pressure-induced stretching of the substrate aimed to recapitulate the dynamic appearance of drusen [10–12]. However, these approaches constrain the *in vitro* system by imposing unphysiological substrate stiffness (MPa range), acute time scale of changes (minutes to hours), and fixed topography.

To address this limitation, we revisited the use of photodegradable hydrogels[13,14] as a tissue culture substrate, providing a platform to study the impact of ECM topographical changes on tissues. As a proof of concept, we applied this system to mimic medium- and large-sized drusen and investigated their impact on stem cell-derived RPE. Through qualitative and quantitative analyses, we demonstrated the impact of this methodology,

which can induce adaptation of the epithelium on a relevant timescale, suggesting mechanobiological insights with implications for the pathophysiology of retinal degeneration. In conclusion, this work highlights the potential of such a tunable hydrogel system, which can be employed in both two-dimensional and three-dimensional setups to investigate the impact of ECM changes over time and length scales comparable to those *in vivo*.

Results and Discussion

Engineering a phototunable hydrogel to dynamically mimic ECM topographical changes in space and time

As ECM remodeling occurs at specific times and length scales, we aimed to develop a tunable hydrogel platform with a photo-degradable mesh. This would allow us to tune its properties in alignment with the *in vivo* situations. To achieve this, we took inspiration from the work of Kloxin and colleagues[13,14]. We synthesized the photodegradable crosslinker (PDC) containing a linear polyethylene glycol (PEG) core, ortho nitro-benzyl groups as photolabile moieties, and acrylate end groups. The PDC was incorporated in PEG-acrylate-based network through a free radical polymerization initiated by a redox reaction of Ammonium persulfate (APS) and Tetramethylethylenediamine (TEMED) (Fig. 1A). The ratio of the different hydrogel precursor components determines the final material properties of the hydrogel, allowing for the tuning of substrate stiffness to mimic *in vivo* ECM mechanical properties. Furthermore, the ratio of PDC and non-degradable PEG components sets the sensitivity of the hydrogel to light. In fact, ortho nitro-benzyl groups are excited by near-UV light (~275-405nm)[13,14], and undergo photolysis, resulting in bond breakage at the benzyl positions, which leads to a partial reduction in mesh size density within the hydrogel structure. As a consequence, an influx of water will result in swelling of the hydrogel (Fig. 1A, B). The simplicity of its implementation is exemplified using a standard inverted microscope, equipped with a 385 nm light-emitting diode (LED), with adjustable intensity and exposure time. Furthermore, the illuminated patterns can be modified by adjusting the stage position, the objective magnification, and the degree of diaphragm opening located between the LED and the objective revolver (Fig. 1B). Interestingly, we found that localized illumination causes local swelling, which in turn leads to topographical changes of the hydrogel surface. These changes can be produced in specific patterns, such as arrays (Fig. 1C), and can be adjusted for swelling by varying the LED intensity or exposure time (Fig. 1D). Next, curious to understand the effect of such changes on the local mechanics, we illuminated areas with diameters of 100 and 300 µm. This resulted in surface bulges with an average height of approximately 20 µm (Fig. 1E). The stiffness of the resulting bulges was then assessed by nanoindentation using a spherical tip with 20 µm diameter and the Effective Young's modules was quantified for a cell-relevant indentation depth of 3.5 µm[15]. To our surprise, the Effective Young's modulus for the -illuminated areas was comparable to that of both non-illuminated areas

of the photodegradable hydrogel and illuminated non-degradable control PEG hydrogel (Fig. 1F). In conclusion, we successfully adapted the use of the PDC to create a substrate, allowing for controllable substrate deformations or topographical changes without significantly changing its stiffness.

To support cell adhesion and bioactivity, hydrogel surfaces typically require functionalization with extracellular matrix proteins or adhesion ligands. In comparison to common cell culture substrates such as plastic surfaces, glass, or polydimethylsiloxane (PDMS), where protein can mostly be deposited by physisorption, the bio-functionalization of PEG hydrogels is primarily achieved by chemisorption using UV-initiated surface activation[16–18]. Since photodegradable hydrogels cannot utilize UV-driven post-functionalization strategies, we developed an alternative strategy. This strategy focuses on an orthogonal reaction route to address the lack of free acrylates after gel polymerization, which are necessary for secondary functionalization reactions. 2-aminoethylmethacrylamide (AEMA) was copolymerized into the polymer backbone, resulting in free amine groups that can be exploited in a post-functionalization step (Fig. 1G). The post-functionalization was achieved by the addition of glycidyl methacrylate (GMA) to access the free amines in the hydrogel and convert them into meth-acrylate groups through an amine-epoxy ring-opening reaction (Fig. 1G, step I). These new acrylates can be further accessed through free radical polymerization with GMA and the branching agent tetramethyl acrylate to build short amine-reactive polymer chains on the surface of the hydrogel (Fig. 1G, step II). Finally, the hydrogel can be incubated with a mixture of the desired adhesive proteins (e.g., basement membrane proteins such as laminins and collagen IV) for 24 hours at 37°C in a standard cell culture incubator. After a sterilization step with an antibiotic mixture, the gels can be successfully used to support cell adhesion and maturation (Fig. 1G, steps III-V).

Overall, we have now optimized a production and coating strategy of a light-tunable platform to mimic and study the impact of ECM deformation on a given biological system in vitro.

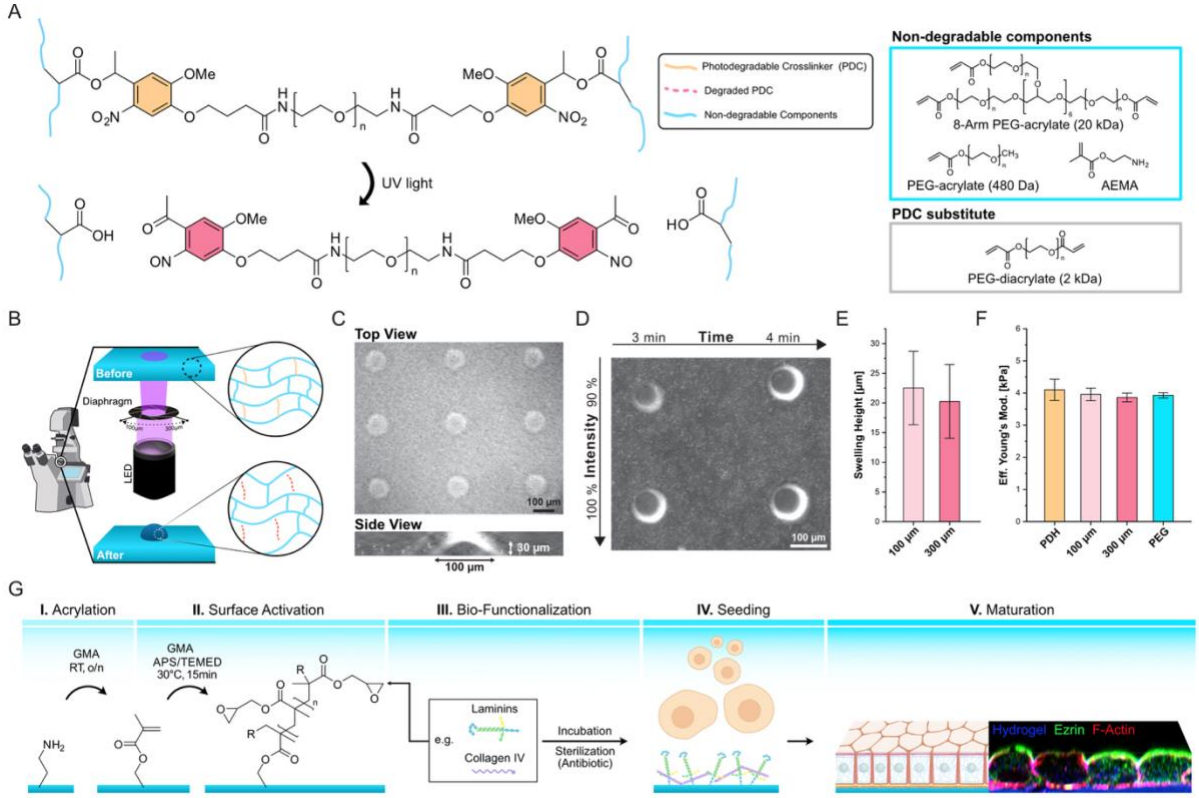

Figure 1: A photodegradable hydrogel to mimic ECM remodeling in relevant time and length scale. A) Photodegradable crosslinker (PDC) connected to non-degradable components of the hydrogel undergoes photolysis after illumination with blue (385nm) light, reducing the crosslinking density. The PDC is incorporated in a non-degradable PEG network composed of 8-Arm PEG-acrylate, PEG acrylate, and AEMA. For a non-degradable hydrogel control, a PEG diacrylate is employed. **B)** Schematic of the experiment setup on an inverted microscope for spatially controlled illumination using an inverted microscope equipped with 385 nm LED and an adjustable diaphragm. **C)** Array patterned to show ease of use and controllability. **D)** Time/Intensity matrix to highlight the potential and versatility of the substrate. **E)** Average swelling height ± SEM of localized illumination of photodegradable hydrogels with a diameter of 100 and 300 µm. **F)** Average Effective Young's modulus ± SEM of the non-illuminated photodegradable hydrogel (PDH), illuminated with a diameter of 100 or 300 µm, and non-degradable PEG control (PEG). Data from E and F were collected from at least three independent experiments, and their statistical significance was assessed using a t-test and one-way ANOVA, respectively. **G)** Illustrated bio-functionalization steps starting after the production of the hydrogels. I) incubation with GMA overnight at room temperature; II) Free radical polymerization of a GMA solution for 15min at 30°C; III) Surface functionalization with a protein mixture overnight at 37°C, followed by sterilization with antibiotic solution; IV) Cell seeding; V) Maturation. The schematic shows an example of a polarized epithelium.

The photodegradable hydrogel enables the controlled investigation of age-related ECM deformation in a stem cell-based RPE model.

To demonstrate the applicability of our photodegradable hydrogel system, we aimed to investigate the impact of substrate topographical deformation on stem cell-derived RPE as a model for studying the correlation between drusen size and the RPE phenotypical switch. We recently demonstrated that this model reliably investigates RPE mechanobiology, as it recapitulates key features of mature human tissue, including its polarization and postmitotic nature[19,20]. Stem cell-derived RPE were able to form continuous monolayers on flat photodegradable hydrogels of 4 kPa in stiffness, coated with a mixture of basement membrane laminins and collagen type IV, thus simulating the biochemical and physical cues of an adult Bruch's membrane[19]. The photodegradable hydrogels were then illuminated to induce local substrate bulging of a diameter of 100 or

300 µm to simulate medium- and large-sized drusen[8] (Fig. 2A). To generate the artificial drusen, selected areas were illuminated for 60 seconds at 3.83 mW/cm^2, reaching complete swelling only after 24 hours of incubation. This gradual change implied minimal acute mechanical stress on the epithelium, thereby more accurately mimicking *in vivo* topographical alterations. To assess the potential impact of UV phototoxicity, RPE monolayers were obtained on PEG hydrogels synthesized using the PDC substitute and also exposed to UV light for 60 seconds at 3.83 mW/cm^2. To assess apicobasal polarity of RPE, we stained for Ezrin, a specific marker for apical microvilli[21,22]. The qualitative evaluation of the high-resolution staining revealed no significant difference between cells on the artificial drusen and the controls, indicating that neither deformation nor UV illumination had a major effect on cell polarity (Fig. 2B). Next, we looked at actin cytoskeleton organization revealing that cells directly atop the artificial drusen showed no obvious morphological differences compared to control regions, with normal actin belt and cortical distribution. However, a close examination of the orthogonal projections of the monolayers suggested changes in monolayer height across the artificial drusen region, both 100 µm and 300 µm in size (Fig. 2C).

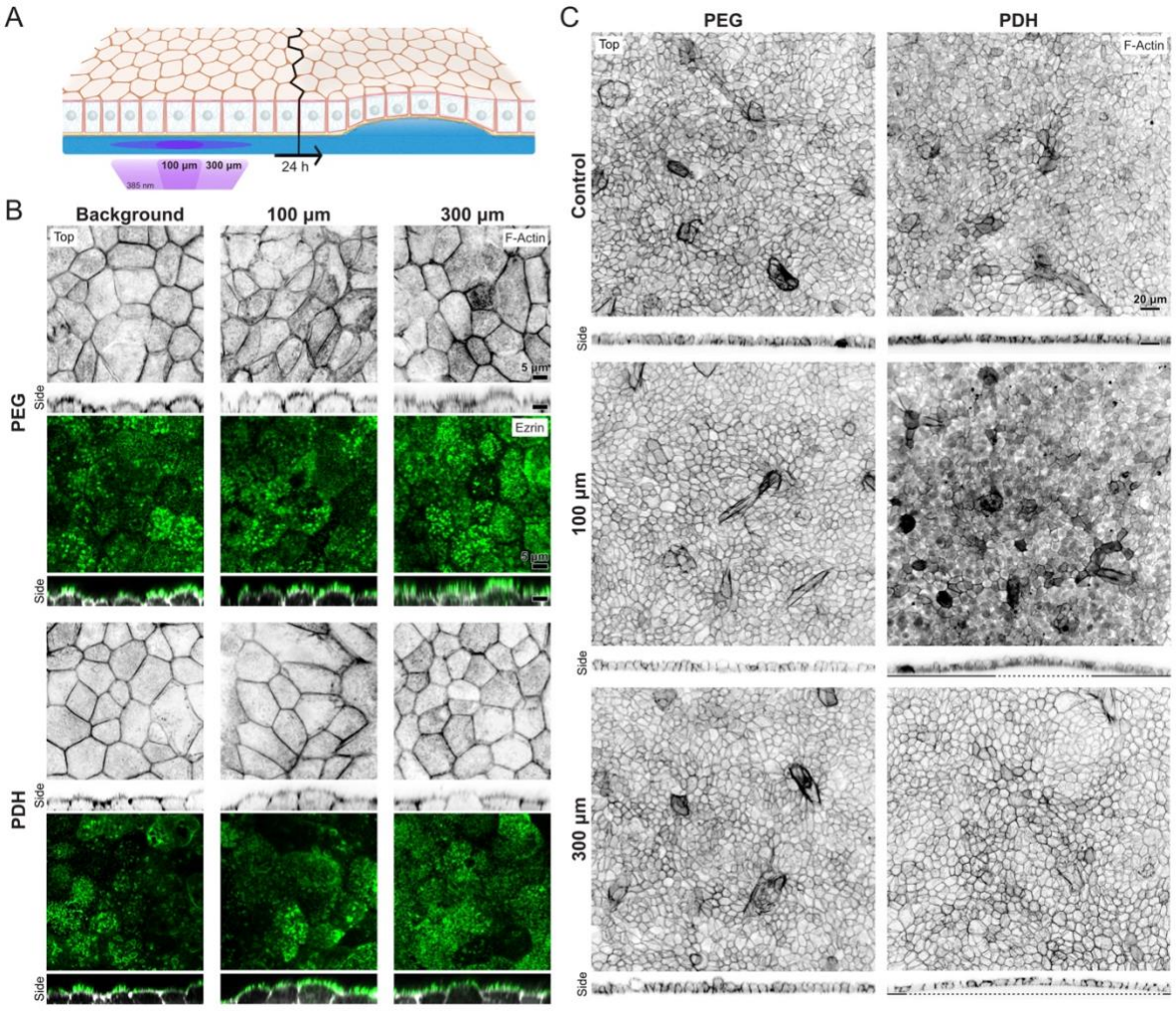

Figure 2: Qualitative characterization of RPE adaptation to artificial drusen at monolayer scale. A) Schematic overview of the dynamic formation of an artificial Drusen. **B)** Representative images of top and orthogonal side views of RPE on illuminated and non-illuminated controls and artificial drusen stained for F-actin and Ezrin. **C)** Overviews of RPE

monolayers stained for F-actin and orthogonal side views obtained on photodegradable hydrogels (PDH) or PEG hydrogels, with or without illumination of a 100 µm and 300 µm diameter area. Dotted lines indicate the diameter of the illuminated regions.

To quantitatively compare tissue-scale implications of artificial drusen induction, the obtained bulges in the monolayers were analyzed in three distinct regions (Fig. 3A). The first region, termed "*Top*" (T), extended radially from the center up to 25 µm for both conditions. The second region, called "*Edge*" (E), was defined as extending 25 µm radially inwards from the respective illumination diameters on the artificial drusen. Lastly, the "*Outside*" (O) region was selected between 150 and 175 µm from the center of the artificial drusen, ensuring that it was not influenced by the surface deformation. Orthogonal views of F-actin-stained RPE monolayers were analyzed to determine monolayer thickness across different regions. The apical and basal cell sides were identified by intensity of signal in line plots (Fig. 3B). The normalized results showed that 100 µm drusen resulted in an average increase in RPE height of approximately 5% at the *Top* and 3% at the *Edge* regions compared to the *Outside* areas, non-illuminated control, and illuminated PEG control. In contrast, the presence of 300 µm large artificial drusen led to a decrease in RPE thickness of about 5% at the *Top*, while the *Edge* region remained unchanged compared to the *Outside* and controls (Fig. 3C). Overall, this means that while the cells on top of the 100 µm artificial drusen are taller, in the same region on 300 µm artificial drusen, the cells become shorter, suggesting that medium-size Drusen "relaxes" the RPE monolayer, whereas the larger Drusen "stretches" the monolayer at the Top region.

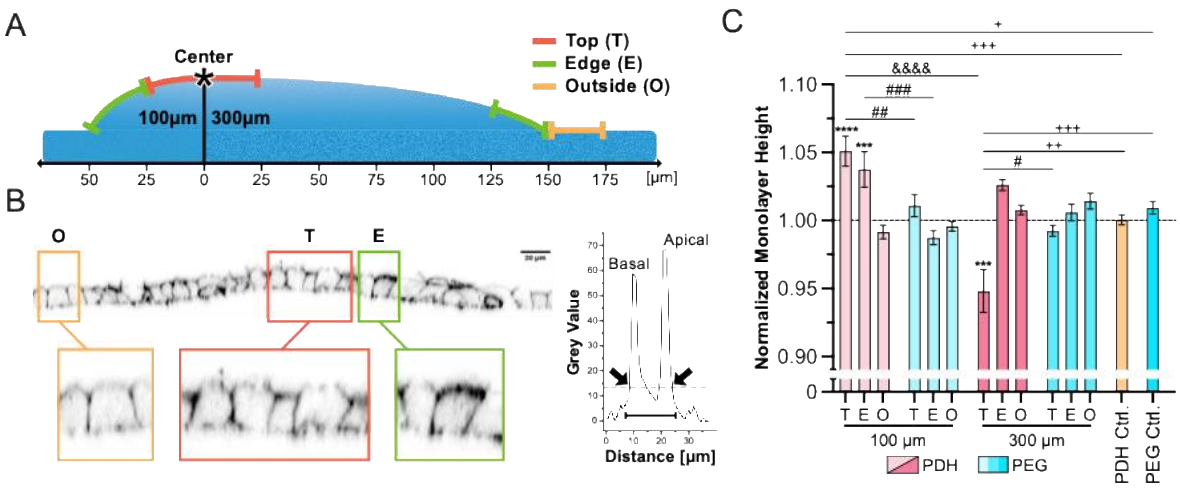

Figure 3: Quantitative characterization of RPE monolayer thickness adaptation to artificial drusen. A) Schematic representation of the division of the regions from the center of the illuminated region (*) employed in the analyses. 100 µm illumination is divided into *Top* 0-25 µm and *Edge* 25-50 µm. 300 µm illumination is divided into *Top* 0-25 µm and *Edge* 125-150 µm. For both conditions, the *Outside* region is defined as 150-175 µm. **B)** Representative orthogonal view of a 100 µm artificial Drusen with three regions highlighted. The profile of the line plot shows the grey value over the distance. Two peaks indicate the basal and apical actin signal. The dashed line indicates the average grey value of the profile, and the arrows show the points the script recognizes as apical and basal delimitators. Finally, the monolayer height is determined as the difference between the two points. **C)** Bar plot showing the average RPE height ± SEM on four illuminated hydrogels in the three regions *Top (T)*, *Edge (E)*, *Outside (O)* and the two controls *Outside* regions. Data were normalized to the average monolayer height of each respective sample and obtained from three to five

independent experiments. Statistical comparison within regions of the illuminated hydrogels is indicated by *, between illuminated PDH and illuminated PEG is indicated by #, comparison between 100 µm and 300 µm illuminated PDH is indicated by &. Finally, comparison between illuminated PDH with PDH and PEG controls by +. Statistical analysis was performed using unpaired two-way ANOVA, where *, #, & or + are $p<0.05$; **, ##, && or ++ are $p<0.01$; ***, ###, &&& or +++ are $p<0.001$; ****, ####, &&&& or ++++ are $p<0.0001$.

Next, we quantified the average cell area and shape factor ($P/\sqrt{A}$) in the different regions. The shape factor is a metric used to characterize the mechanical state of epithelial tissues, where higher values reflect an increased influence of cell-cell adhesion and unjamming, whereas lower values reflect greater cortical tension and a jammed homeostatic state [23]. The lateral outline of the cells was determined by the maximum projection of the tight junction signal ZO-1 (Fig. 4A, Sup. Fig. 1A). A comparison of the average cell areas and shape factors revealed no significant differences between the conditions (Sup. Fig. 2), excluding major monolayer unjamming induced by the drusen. Nevertheless, the data showed notable variability and emerging trends in cell area, suggesting the presence of different subpopulations. To investigate this further, we analyzed the frequency distribution of the quantified values. Interestingly, the frequency curve of cell areas for the 100 µm artificial drusen revealed a bimodal behavior for the cells at the *Top* region, a pattern not observed for the *Top* region of the RPE on 300 µm large artificial drusen (Fig. 4B and C). In fact, a more unimodal distribution was found in this condition, in the controls and at the *Edge* and *Outside* areas of both drusen size (Sup. Fig. 3). The difference in area distribution supports the hypothesis that a change in the organization of the monolayer may be caused by the disruption of an existing force balance, which induces a topological shift in RPE on 100 µm artificial Drusen, but not on 300 µm artificial Drusen.

Following this logic, we analyzed cellular orientation as a proxy for assessing the mechanical continuum in epithelia, given that epithelial cells typically align with maximum average stress [24–26]. We quantified the relative orientation of the cells in relation to the center of the artificial drusen by calculating the scalar product between the absolute angle of the cell and the angle directed towards the center of the artificial drusen (Sup. Fig. 1B). This angle varies from 0° to 90°, indicating alignment towards the drusen's center or orthogonal positioning, respectively (Fig. 4D). While we could not observe any clear orientation pattern in RPE cells on 300 µm drusen and controls, we identified a significant circular oritenation along the 100 µm drusen *Edge* region (Fig. 4D and E). This response can be described as a ring forming around the artificial drusen, separating the inner *Top* region from the *Outside* region. In contrast, for the 300 µm artificial drusen, we observed a less prominent response in the *Top* region, where cells showed a tendency to align towards the center.

Overall, our data showcase the importance of time (24 hours swelling) and space (100 vs. 300 µm) control in mimicking ECM topographical deformation when studying RPE phenotypical changes. In contrast to more acute systems[10,12], here the RPE monolayers

adapt to ECM bulging in a manner more akin to *in vivo* conditions, without the immediate and extreme loss of polarity or integrity seen with acute or non-physiological deformations. Instead, the quantified differences in mechanical stress on 300 µm artificial drusen, which are inferred by monolayer thinning, may provide mechanobiological insights into the pathophysiology of the RPE phenotypical switch observed *in vivo*.

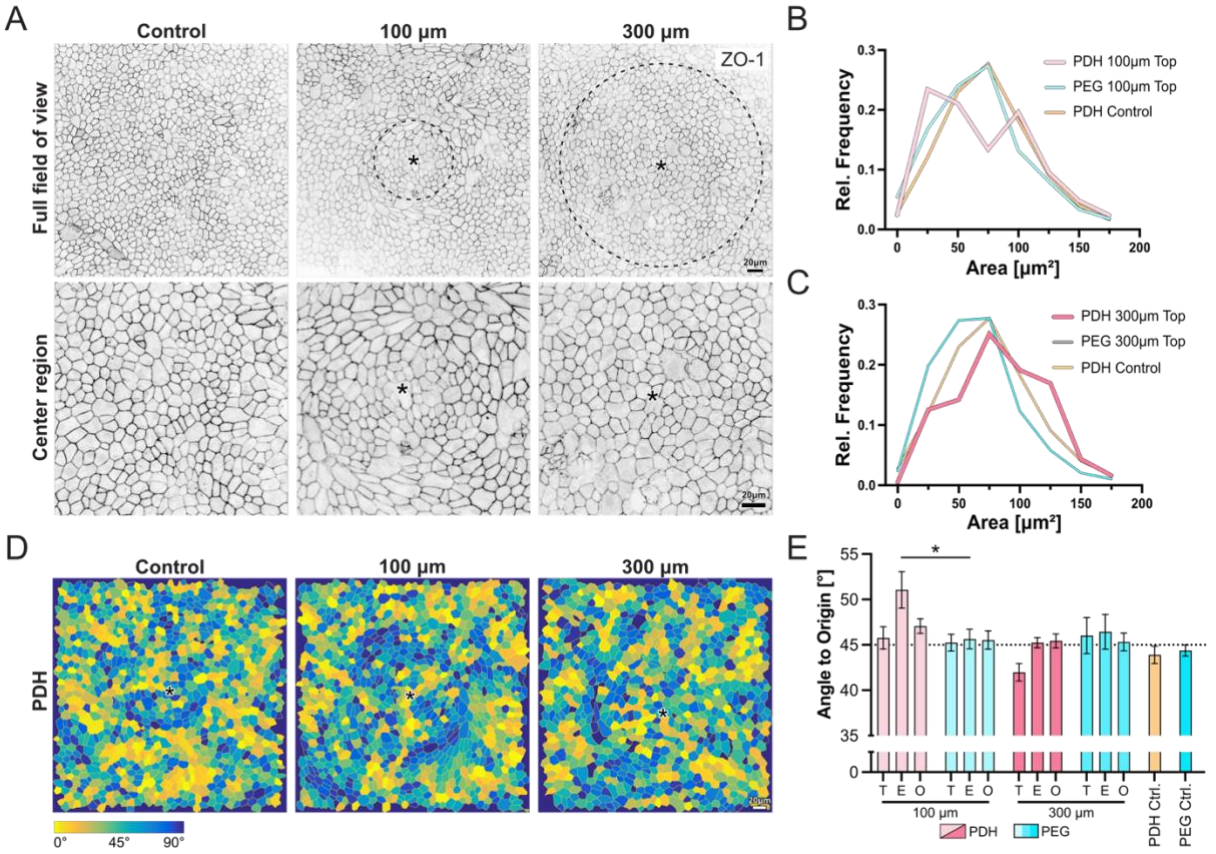

Figure 4: Morphometric characterization of RPE adaptation to artificial drusen at a cellular scale. A) Representative overviews (top) and magnifications (bottom) of RPE monolayers stained for ZO-1 on photodegradable hydrogels (PDH) with or without illumination. The illuminated areas are indicated by a dashed line. **B, C)** Relative frequency distributions of the cell areas for *Top* regions of 100 µm (B) and 300 µm (C) artificial drusen, non-illuminated control. **D)** Representative color-coded maps of angular orientation of RPE cells with respect to the drusen center. In yellow is indicated 0° angle towards the center of artificial Drusen (or center of the picture for the control), and in dark blue 90° angle, indicating a perpendicular orientation (Left). **E)** Bar plot of the average cell orientation angle to origin ± SEM quantification for the four illuminated conditions and non-illuminated controls (Right). Statistical analysis was performed using unpaired two-way ANOVA, where * is $p<0.05$.

Conclusion and Outlook

In this study, we optimized a photodegradable hydrogel that can be tailored to achieve physiologically relevant stiffness and on-demand dynamic deformation. Additionally, we developed a bio-functionalization protocol that creates a defined surface coating without relying on UV light. Our results demonstrated successful cell attachment and the formation of a monolayer of stem cell-derived RPE cells. Furthermore, we were able to induce dynamic changes in the topography of the substrate on demand, with variations

in two different sizes, simulating ECM deformation (drusen) as a characteristic of retinal aging. Changes in hydrogels were observed within 24 hours, enabling the adaptation of the epithelial monolayer. This allows for the investigation of a progressive age-mimicking response that is distinct from acute reactions.

Using this system, we found that the multicellular response varies with the size of the induced swelling, resulting in distinct differences in monolayer adaptation in terms of height and cell morphology, specifically cell area and orientation, without altering cellular polarization, as highlighted by Ezrin staining. These findings suggest that larger deformations are creating higher mechanical stress on the monolayer, which can eventually lead to the loss of cellular polarity in combination with other environmental stresses. On the other hand, medium-sized deformations induce cellular reorganization that may protect cells from mechanical stress and loss of polarity. Interestingly, this is consistent with the higher probability of large drusen to induce retinal degeneration compared to medium-sized drusen [8,9]. Specifically, smaller disruptions are less likely to induce retinal degeneration; however, crossing an unknown threshold appears to have more significant effects on retinal health and vision.

This work has yielded exciting new insights into a challenging-to-study pathology and can serve as a starting point for further research on mechanobiology aspects of retinal degeneration. Most importantly, the relevant substrate stiffness and temporal scale of the changes have not dramatically disrupted the monolayer polarity, as seen in more acute substrate deformation models[12]. This supports the significance of our system for modelling relevant aging phenomena. Moreover, the versatility of the photodegradable hydrogel enables future work to focus on the development of drusen over time and their density changes, combined with more complex bioengineered tissue equivalents, such as organoids.

Overall, this photodegradable hydrogel has potential for diverse model systems, as its initial bulk stiffness and protein functionalization can be precisely tuned to replicate the ECM of the target tissue. Moreover, its post-illumination mechanical properties and topographical features can be finely adjusted by modifying the hydrogel composition. The ability to control illumination patterns adds another level of versatility, enabling researchers to dynamically mimic ECM remodeling in both time and space at length scales relevant to tissue developmental, age-related, and mechanobiological processes.

Methods

Photodegradable crosslinker synthesis

The synthesis of the photodegradable crosslinker (PDC) followed the published work from Kloxin et al.[14]. Briefly, under an inert atmosphere, 4-(4-(1-Hydroxyethyl)-2-methoxy-5-nitrophenoxy)butanoic acid (Iris Biotech) was dissolved in dry dichloromethane (Carl Roth, No.1A9K.1) and deprotonated by triethylamine (Sigma Aldrich, 471283). After cooling the reaction mixture in an ice bath, Acryloyl chloride (Sigma Aldrich, A24109-100G) was added dropwise. After complete addition, the ice bath was removed, and the reaction mixture was stirred at room temperature overnight, then poured into water and a liquid-liquid extraction with chloroform was performed. The organic phase was dried to yield 4-(4-(1-(acryloyloxy)ethyl)-2-methoxy-5-nitrophenoxy)butanoic acid. Its purity was confirmed using nuclear magnetic resonance analysis. In the final step of the reaction, 1-Hydroxybenzotriazol hydrate (HOBt - Sigma Aldrich, 54802-10G-F) and 2-(1H-Benzotriazole-1-yl)-1,1,3,3-tetramethylaminium hexafluorophosphate (HBTU - Sigma Aldrich, 8510060025) were dissolved in N-Methyl-2-pyrrolidone (Sigma Aldrich, 443778), then activated with N, N-Diisopropylethylamine (Sigma Aldrich, 387649). After 5 minutes, PEG-bis amine (Biopharma PEG, HO005005-2K) in N-Methyl-2-pyrrolidone was added, and the mixture was stirred for 24 hours. The reaction mixture was then precipitated in cold diethyl ether, centrifuged, and the resulting brown paste was resuspended in water and dialyzed against five liters of water for three days, with the water changed twice daily. After lyophilization, the product was obtained as a brown solid and purity was checked by nuclear magnetic resonance and electrospray ionization mass spectrometry.

Hydrogel synthesis

To covalently bond the gel to the glass surface the glass bottom dishes (Cellvis, D35-20-0-N) were activated with 3-(Trimethoxysilyl)propylmethacrylat (abcr, AB109006) with an adapted protocol from Sigma Aldrich (Sigma Aldrich, M6514). Here repeated in short: The glass surface was activated by O_2 plasma for 1 min at 200 W in a plasma oven. A 3-(Trimethoxysilyl)propylmethacrylat ethanol solution was mixed with diluted acetic acid to allow methanol as a leaving group after the nucleophilic attack of the activated glass surface to the silane. The activated reaction mixture was transferred into the glass bottom dish and the surface functionalization proceeded for three minutes. Afterwards, the dishes were washed with distilled water and ethanol and put in the oven for 15 min at 60°C to evaporate the remaining washing solvents.

PDMS rings with an inner diameter of 4 mm and height of 200 µm (Darwin Microfluidics, DM-S-PDMS-200) were placed on activated glass bottom dishes. The gel solution was prepared by sequential addition of the components. For the photodegradable gels with an Effective Young's modulus of 4 kPa the composition was as follows: Poly(ethylenglycol)methyletheracrylat (10 µL, 100 mM, 556 eq., Sigma Aldrich, 454990-250ML), 2-Aminoethylmethacrylat -hydrochlorid (10 µL, 7.55 mM, 5 eq., Sigma Aldrich,

516155-5G), PDC (22.5 µL, 75 mM, 112 eq.), 8-Arm PEG-Acrylate (1.5 µL, 10 mM, 1 eq., Biopharma PEG, A88009-20K), Ammonium persulfate (APS) (4 µL, 1.97 M, Sigma Aldrich, 248614-5G) and lastly N,N,N',N'-Tetramethylethylenediamine (TEMED) (2 µL, 1.98 M, Sigma Aldrich, 411019-100ML). All the monomers amounted to 17.6 wt/vol%. The composition for the non-degradable gels with an effective Young's modulus of 4 kPa the composition was adjusted to: Deionized water (20 µL), Poly(ethylenglycol)methyletheracrylat (10 µL, 100 mM, 556 eq.), 2-Aminoethylmethacrylat -hydrochlorid (10 µL, 7.55 mM, 5 eq.), Poly(ethylene glycol) diacrylate (22.5 µL, 100 mM, 150 eq. Sigma Aldrich, 701971-1G), 8-Arm PEG-Acrylate (1.5 µL, 10 mM, 1 eq., Biopharma PEG, A88009-20K), APS (1 µL, 1.97 M), TEMED (0.5 µL, 1.98 M). After the addition of APS and again after the addition of TEMED the reaction mixture was vortexed and shortly spun down to ensure homogeneous distribution of all the monomers and initiators. Roughly 15 µL gel solution was pipetted into the PDMS rings, covered with a Teflon disc, and transferred onto a heater set to 30°C for temperature-controlled polymerization for 1 hour. Afterwards, the gels were flipped upside down for an additional 20 min to ease Teflon-disc detachment, which was promoted by 5 min sonication. The hydrogels were immediately used for the next steps or stored in the dark for a maximum of 12 hours in distilled water at room temperature.

Nanoindentation

The Effective Young's modulus of the photodegradable and non-degradable gels was measured by nanoindentation, using a Chiaro Nanoindenter (Optics 11 Life). The probe had a 20 µm spherical glass tip and 0.025 N/m cantilever stiffness. The samples were indented using displacement mode with a maximum depth of 3.5 µm. Analysis of the indentation data was performed in the Optics 11 analysis software (DataViever V2, version 2.6.3) following the Hertz contact model fitting while using single fit mode up to 100% of Pmax and filtering values for a R^2 greater than 0.95.

Hydrogel functionalization

The hydrogels were incubated with a Glycidyl methacrylate (GMA) solution (75 µM, Sigma Aldrich 151238-100G) overnight. After removing the unreacted GMA the functionalization solution consisting of: 590 µL H2O, 3uL GMA, 10 µL Di(trimethylolpropane) tetraacrylate (TMA) (0.2 vol/vol% in EtOH, Sigma Aldrich, 408360-100ML), 10uL APS (1.97 M), 2.5 µL TEMED (1.98 M) was added on top of the hydrogels and the gels were put on a heating plate at 30°C, 15min for photodegradable gels and 10 min for non-degradable gels. Directly afterwards the excess poly-GMA was washed off and one by one a hydrophobic barrier with an inner diameter of 6 mm was placed around the gel and immediately the protein solution consisting of: 38.5 µL PBS, 7.5 µL Laminin-332 (100ug/mL, Biolamina, LN332), 7.5 µL Laminin-511 (100 ug/mL, Biolamina, LN511) and 1.5 µL Human Collagen type IV (30 µg/mL, Sigma-Aldrich, C7521-10MG) was pipetted onto the gel. Lastly, the dishes were placed in a cell culture incubator overnight and before use sterilized by washing twice with gentamicin solution for 15 min. Hydrophobic barriers with an inner

369 diameter of 4mm were placed around the sterilized gels and a bubble of 30 µL cell culture
370 medium was placed on top of the gels.

371 **Cell culture**

372 Before seeding the human induced pluripotent stem cell-derived RPE cells (Fujifilm
373 Cellular Dynamics, R1102) on the hydrogels, the culture was expanded for a week on
374 vitronectin XF (2.5 µg/mL, 440µL, StemCell technologies, 07180) coated 24- well plates
375 as previously reported[19]. The medium composition followed a scaled up version of the
376 manufacturer's instructions; in short it contained MEM-alpha with nucleosides (273.9
377 mL, Thermo Fisher, 12571063), 100x Glutamax (2.79 mL, Thermo Fisher, 35050061),
378 KnockOut Serum replacement (15 mL, Gibco, 10828028), N2-Supplement (3 mL, Gibco,
379 17502048), Hydrocortisone (0.33 mL, 50 µM, Sigma Aldrich, H6009), Taurine (1.5 mL, 50
380 µg/mL, Sigma Aldrich, T8691), Triiodo-L-thyronine (0.21 mL, 20 ng/mL, Sigma Aldrich,
381 T5516) and Gentamicin (0.15 mL, 50 mg/mL, Gibco, 15750060); and medium changes
382 were performed every two days. To generate a single cell solution necessary for seeding
383 on hydrogels the cells were detached by 30 min incubation with 5 mM PBS/EDTA (Sigma
384 Aldrich, E6511), followed by a gentle mechanical wash and finished by a 5 min incubation
385 with TrypLE Express (Gibco, 126050). A final concentration of 2.5 million cells/mL was set
386 and 30µL of cell suspension was used per gel. The cells attached overnight and on the
387 next day 1.5 mL of medium was added to the dish. The culture was maintained for a week
388 with two medium changes.

389 **Artificial Drusen formation**

390 The illumination was performed on a Zeiss Axio Observer 7 with incubation and CO_2
391 buffering. Using a 20x objective and a LED diode with 3.83mW/cm^2 at 100% intensity of
392 the 385 nm channel. The size of the artificial drusen was regulated by opening or closing
393 the diaphragm of the Zeiss Axio Observer and calibrated for each condition. Multiple
394 positions were set, ensuring sufficient spacing to prevent overlap of interference between
395 regions. Additionally, the focal plane was set to 50 µm below the cell monolayer, within
396 the gel. Afterwards, the positions were illuminated one by one for 60 s (230 mJ/cm^2) and
397 the gels were put back into the incubator. Fixation was performed 24 hours after
398 illumination with 2 w/v% PFA in PBS (Thermo Fisher, J61899.AK) at room temperature for
399 8 min.

400 **Immunofluorescent staining and imaging**

401 The fixed samples were prepared for immunofluorescent staining by incubation with
402 Triton-X-100 (0.3 vol/vol%, Sigma Aldrich, T8787) for 2 min at room temperature. After
403 washing 3 times with PBS unspecific binding of the antibodies was prevented by 30 min
404 1% BSA (Serva, 11930) blocking step. With this, sample preparation was finished and the
405 primary antibodies in blocking solution were added for overnight incubation at 4°C. To
406 remove unbound primary antibodies, the samples were washed three times with PBS
407 before addition of secondary antibodies and incubation for a minimum of 2 hours at room
408 temperature. Lastly, the samples were washed again and finally stored in PBS prior to

imaging. Samples were imaged at a Zeiss LSM710 Confocal Microscope with a 40x water immersion objective (Zeiss, 420862-9970-000) in normal confocal mode (Z-stack 1.1 µm optical slicing) and Airyscan super resolution mode (Z-stack 0.25 µm optical slicing). Image processing and quantification were performed using Fiji software (National Institutes of Health, USA). The following primary and secondary antibodies were employed: mouse anti-human Ezrin (Abcam, ab4069, 10 µg/ml); rabbit anti-human ZO-1 (Thermo Fisher Scientific, 61-7300, 2.5 µg/ml); Alexa Fluor 488 anti-mouse IgG (DRUSEN+L) (Invitrogen, A11001, 8 µg/ml); Alexa Fluor 594 anti-rabbit IgG (DRUSEN+L) (Invitrogen, A11012, 4 µg/ml). Finally, Phalloidin-iFluor 647 dye (Abcam, ab176759, 1:1000) was used to visualize F-actin.

Analysis of monolayer thickness, area, and angle to origin

All measurements were performed by a custom script in Fiji [27]. To quantify the monolayer thickness, the confocal stacks obtained from the F-Actin channel were resliced, and at 10% intervals of the total frame width (with a 5% offset from the frame edge) Intensity line plots were drawn vertically to determine the apical and basal edges of the monolayer. For each line plot, the mean grey value was determined and used to apply a threshold where the F-actin signal rose above the background noise. The monolayer was defined as the vertical distance difference between the apical and basal threshold-crossing points. For better comparability, each value was normalized by the mean of the respective experiment. Furthermore, for each measured value, the distance from the center of the artificial Drusen was calculated. To quantify the average cell area, the confocal stacks obtained in the F-Actin channel were flattened by Z Projection. Cellpose software[28] was then used to determine the cell outlines and measure cell area, shape factor, and distance to the center of the artificial Drusen. For better comparability, each value was normalized by the mean of the respective experiment. To quantify the angle to origin, the absolute angle from the segmented cells in Cellpose was determined. To calculate the "angle to origin", first we measured the distance and drew a vector towards the center of the artificial Drusen. Then, we calculated the scalar product using the vectorized absolute angle.

Declaration of AI use

The preparation of this manuscript has been aided by AI-assisted technologies to improve its readability and language.

Acknowledgment

We would like to acknowledge all the members of the REMeD group in the past years for their contributions to the discussion of the work. Moreover, we appreciate Adam Breitscheidel's technical support in graphic design, Gloria's excellent help in Drusen induction, and Sebastian Pape for the help with the Fuji script.

Fundings

This work in Di Russo's laboratory was supported by the German Research Foundation (DFG; RU 2366/3-1 and 363055819/GRK2415). Furthermore, we would like to acknowledge the financial support from the Exploratory Research Space (ERS) of RWTH Aachen University.

F.R. was supported by a PhD fellowship of the Pro Retina Stiftung, and A.N.K. and T.P. by Add-on Fellowships of the Joachim Herz Foundation.

Author contributions

FR: methodology, software, analysis, investigation, writing, and visualization. CB: methodology. IS: methodology, investigation. TP: investigation. VTK: investigation. AK: investigation. SY: investigation. LDL: supervision, resources. JDR: supervision, resources, funding acquisition, writing, conceptualization, and visualization.

Competing interests

Authors declare that they have no competing interests.

References

[1] P. Lu, K. Takai, V. M. Weaver, Z. Werb, *Csh Perspect Biol* **2011**, *3*, a005058.

[2] A. N. Kozyrina, T. Piskova, J. Di Russo, *Frontiers Bioeng Biotechnology* **2020**, *8*, 596599.

[3] C. Frantz, K. M. Stewart, V. M. Weaver, *J Cell Sci* **2010**, *123*, 4195.

[4] K. B. Jensen, M. H. Little, *Stem Cell Rep.* **2023**, *18*, 1255.

[5] B. Artegiani, D. Hendriks, *Dev. Cell* **2025**, *60*, 493.

[6] E. L. Fletcher, A. I. Jobling, U. Greferath, S. A. Mills, M. Waugh, T. Ho, R. U. de Iongh, J. A. Phipps, K. A. Vessey, *Optom. Vis. Sci.* **2014**, *91*, 878.

[7] S. Chen, N. A. Popp, C.-C. Chan, *Expert Rev. Ophthalmol.* **2014**, *9*, 285.

[8] T. J. Heesterbeek, L. Lorés-Motta, C. B. Hoyng, Y. T. E. Lechanteur, A. I. den Hollander, *Ophthal Physl Opt* **2020**, *40*, 140.

[9] S. M. Waldstein, W.-D. Vogl, H. Bogunovic, A. Sadeghipour, S. Riedl, U. Schmidt-Erfurth, *Jama Ophthalmol* **2020**, *138*, 740.

[10] F. Farjood, A. Ahmadpour, S. Ostvar, E. Vargis, *J. Biol. Eng.* **2020**, *14*, 13.

[11] K. Yamaguchi, T. Matsuo, F. Shiraga, H. Ohtsuki, *Jpn. J. Ophthalmol.* **2001**, *45*, 470.

[12] F. Farjood, E. Vargis, *Lab Chip* **2018**, *18*, 3413.

[13] A. M. Kloxin, A. M. Kasko, C. N. Salinas, K. S. Anseth, *Science* **2009**, *324*, 59.

[14] A. M. Kloxin, M. W. Tibbitt, K. S. Anseth, *Nat. Protoc.* **2010**, *5*, 1867.

[15] A. Buxboim, K. Rajagopal, A. E. X. Brown, D. E. Discher, *J. Phys.: Condens. Matter* **2010**, *22*, 194116.

[16] Y. J. Chuah, Z. T. Heng, J. S. Tan, L. M. Tay, C. S. Lim, Y. Kang, D.-A. Wang, *Colloids Surf. B: Biointerfaces* **2020**, *191*, 110995.

[17] A. Wolfel, M. Jin, J. I. Paez, *Front. Chem.* **2022**, *10*, 1012443.

[18] R. L. Wilson, G. Swaminathan, K. Ettayebi, C. Bomidi, X.-L. Zeng, S. E. Blutt, M. K. Estes, K. J. Grande-Allen, *Tissue Eng. Part C: Methods* **2021**, *27*, 12.

[19] A. N. Kozyrina, T. Piskova, F. Semeraro, I. C. Doolaar, T. Prapty, T. Haraszti, M. Hubert, R. Windoffer, R. E. Leube, A.-S. Smith, J. Di Russo, *EMBO Rep.* **2025**, 1.

[20] T. Piskova, A. N. Kozyrina, G. Astrauskaitė, M. H. E. Mabrouk, S. Schepl, S. L. S. Yam, R. Ravithas, W. Wagner, M. Vassalli, J. Di Russo, *bioRxiv* **2025**, DOI 10.1101/2025.05.22.655517.

[21] V. L. Bonilha, S. C. Finnemann, E. Rodriguez-Boulan, *J. Cell Biol.* **1999**, *147*, 1533.

[22] V. L. Bonilha, M. E. Rayborn, I. Saotome, A. I. McClatchey, J. G. Hollyfield, *Exp. Eye Res.* **2006**, *82*, 720.

[23] D. Bi, J. H. Lopez, J. M. Schwarz, M. L. Manning, *Nat Phys* **2015**, *11*, 1074.

[24] A. Nestor-Bergmann, G. Goddard, S. Woolner, O. E. Jensen, *Math. Med. Biol.: A J. IMA* **2018**, *35*, 1.

[25] D. T. Tambe, C. C. Hardin, T. E. Angelini, K. Rajendran, C. Y. Park, X. Serra-Picamal, E. H. Zhou, M. H. Zaman, J. P. Butler, D. A. Weitz, J. J. Fredberg, X. Trepat, *Nat Mater* **2011**, *10*, 469.

[26] T. P. J. Wyatt, A. R. Harris, M. Lam, Q. Cheng, J. Bellis, A. Dimitracopoulos, A. J. Kabla, G. T. Charras, B. Baum, *Proc. Natl. Acad. Sci.* **2015**, *112*, 5726.

[27] J. Schindelin, I. Arganda-Carreras, E. Frise, V. Kaynig, M. Longair, T. Pietzsch, S. Preibisch, C. Rueden, S. Saalfeld, B. Schmid, J.-Y. Tinevez, D. J. White, V. Hartenstein, K. Eliceiri, P. Tomancak, A. Cardona, *Nat. Methods* **2012**, *9*, 676.

[28] C. Stringer, T. Wang, M. Michaelos, M. Pachitariu, *Nat Methods* **2021**, *18*, 100.

Supporting Information

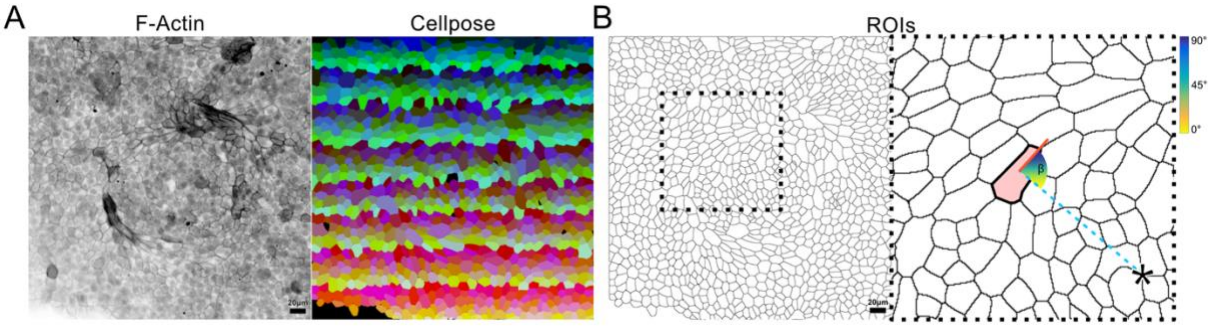

Supplementary Figure 1: Methodology for quantifying cellular angles to the origin. A) Representative maximum intensity projection of F-actin-stained RPE with the Cellpose segmentation output picture. **B)** Representative maximum projection of a ZO-1-stained RPE with the zoomed-in region highlighted by a dashed line. The center of the artificial drusen is marked by an asterisk. The absolute angle of the cell is indicated by the red solid line, while the vector from the center of the highlighted cell to the center of the artificial drusen is indicated by the dotted line. The scalar product between the two vectors is indicated by angle β and lies between 0° and 90°, as shown by a color gradient from yellow to blue.

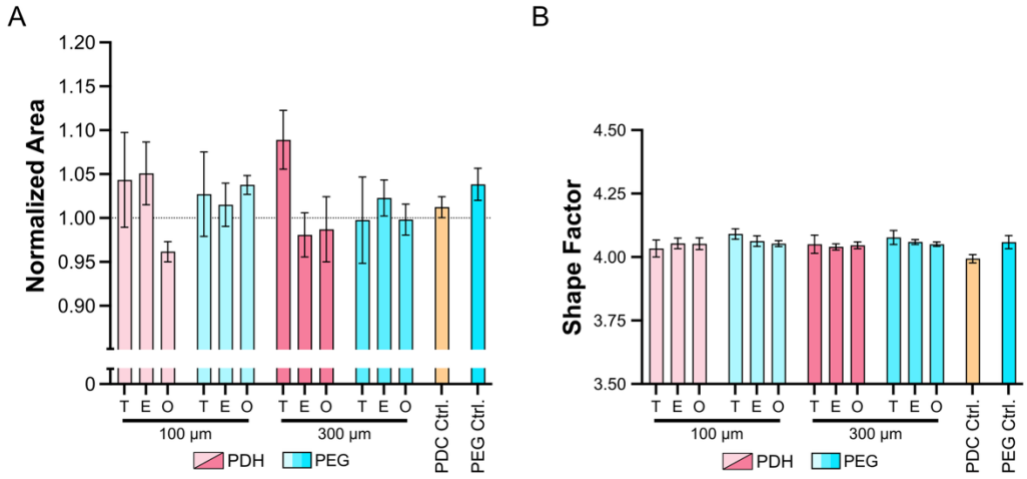

Supplementary Figure 2: RPE cell areas and shape factors. A) Bar plot showing normalized average cell area ± SEM in all conditions. **C)** Bar plot showing the normalized shape factor ± SEM in all conditions**.**

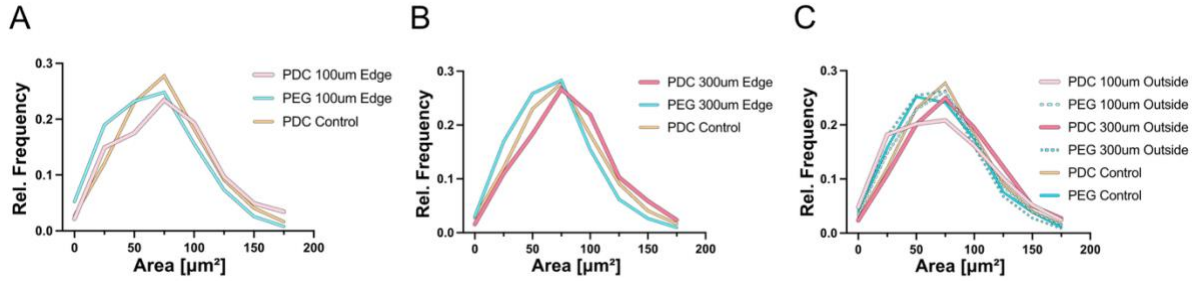

Supplementary Figure 3: Cell area distribution. Relative frequency distributions of the cell areas for RPE on 100 µm Edge (A) and controls, 300 µm Edge and controls (B), and 100 µm, 300 µm Outside and controls (C).

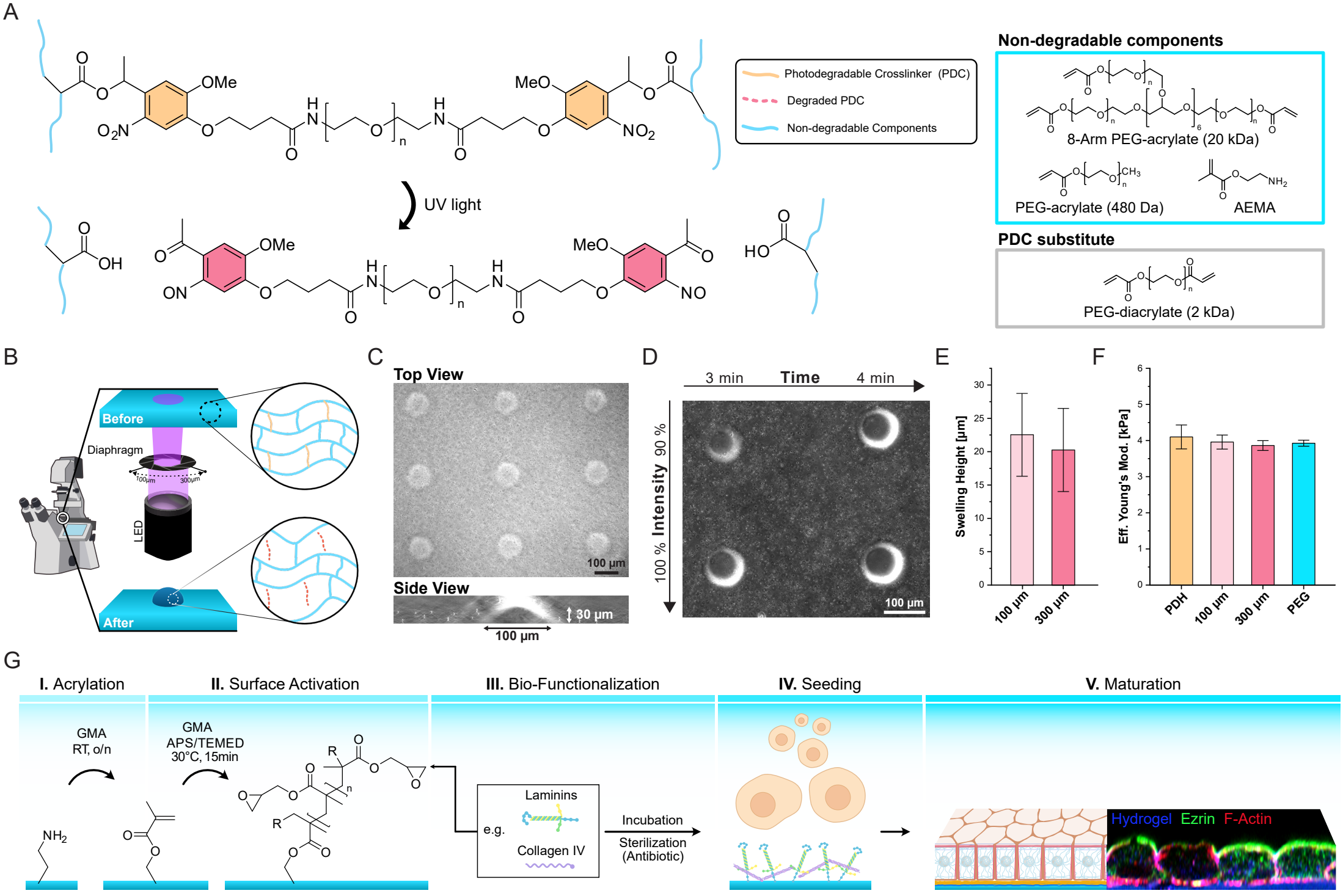
A
Photodegradable Crosslinker (PDC)
Degraded PDC
Non-degradable Components
UV light
Non-degradable components
8-Arm PEG-acrylate (20 kDa)
PEG-acrylate (480 Da)
AEMA
PDC substitute
PEG-diacrylate (2 kDa)
B
Before
After
Diaphragm
LED
C
Top View
Side View
100 µm
30 µm
D
3 min
Time
4 min
100 % Intensity 90 %
E
Swelling Height [µm]
100 µm
300 µm
F
Eff. Young's Mod. [kPa]
PDH
PEG
G
I. Acrylation
II. Surface Activation
III. Bio-Functionalization
IV. Seeding
V. Maturation
GMA
RT, o/n
APS/TEMED
30°C, 15min
e.g.
Laminins
Collagen IV
Incubation
Sterilization
(Antibiotic)
Hydrogel
Ezrin
F-Actin

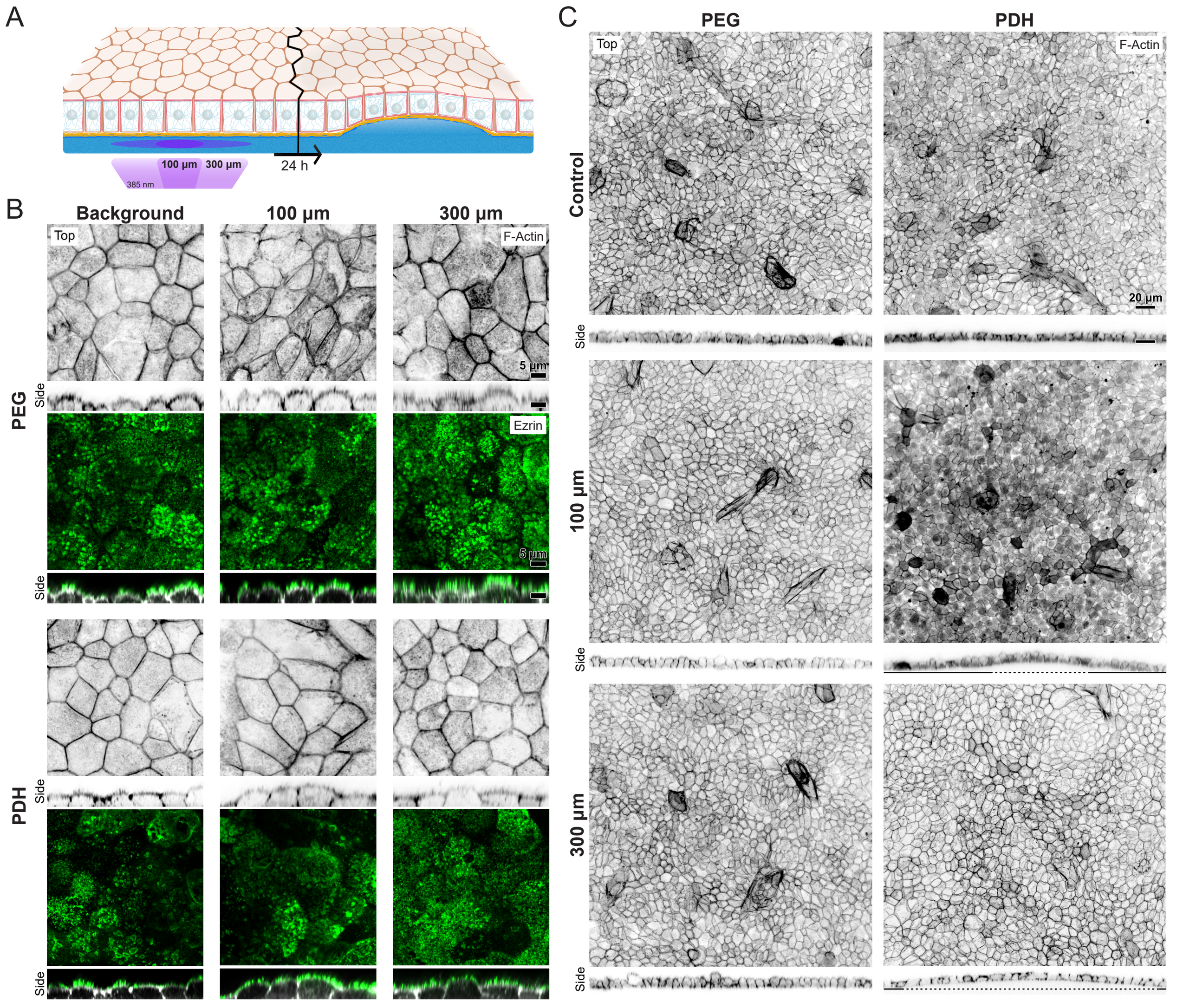
A
100 µm
300 µm
385 nm
24 h
B
Background
100 µm
300 µm
PEG
PDH
Top
Side
F-Actin
Ezrin
5 µm
C
PEG
PDH
Control
100 µm
300 µm
Top
F-Actin
20 µm
Side

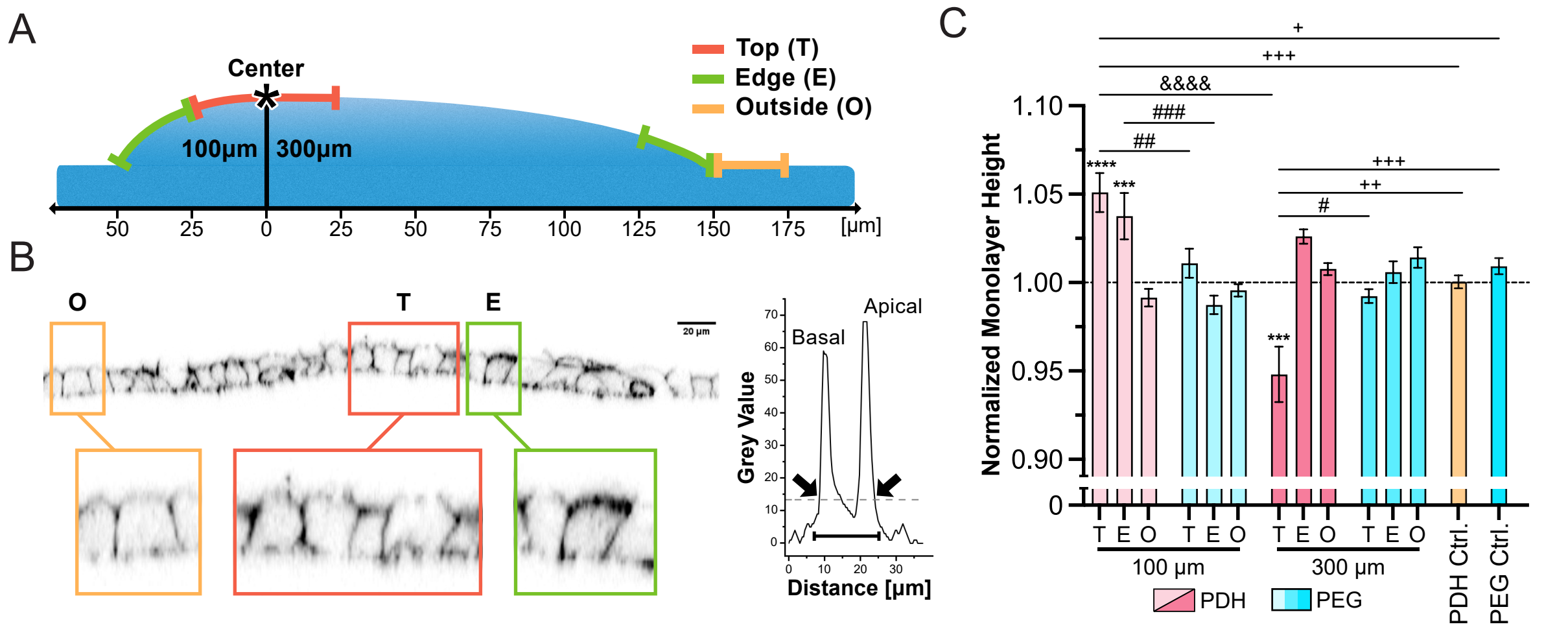
A
Center
Top (T)
Edge (E)
Outside (O)
100µm
300µm
50
25
0
25
50
75
100
125
150
175
[µm]
B
O
T
E
20 µm
Apical
Basal
Grey Value
Distance [µm]
C
Normalized Monolayer Height
1.10
1.05
1.00
0.95
0.90
0
+
+++
&&&&
###
##
++
#
****
***
T E O T E O T E O T E O
100 µm
300 µm
PDH
PEG
PDH Ctrl.
PEG Ctrl.

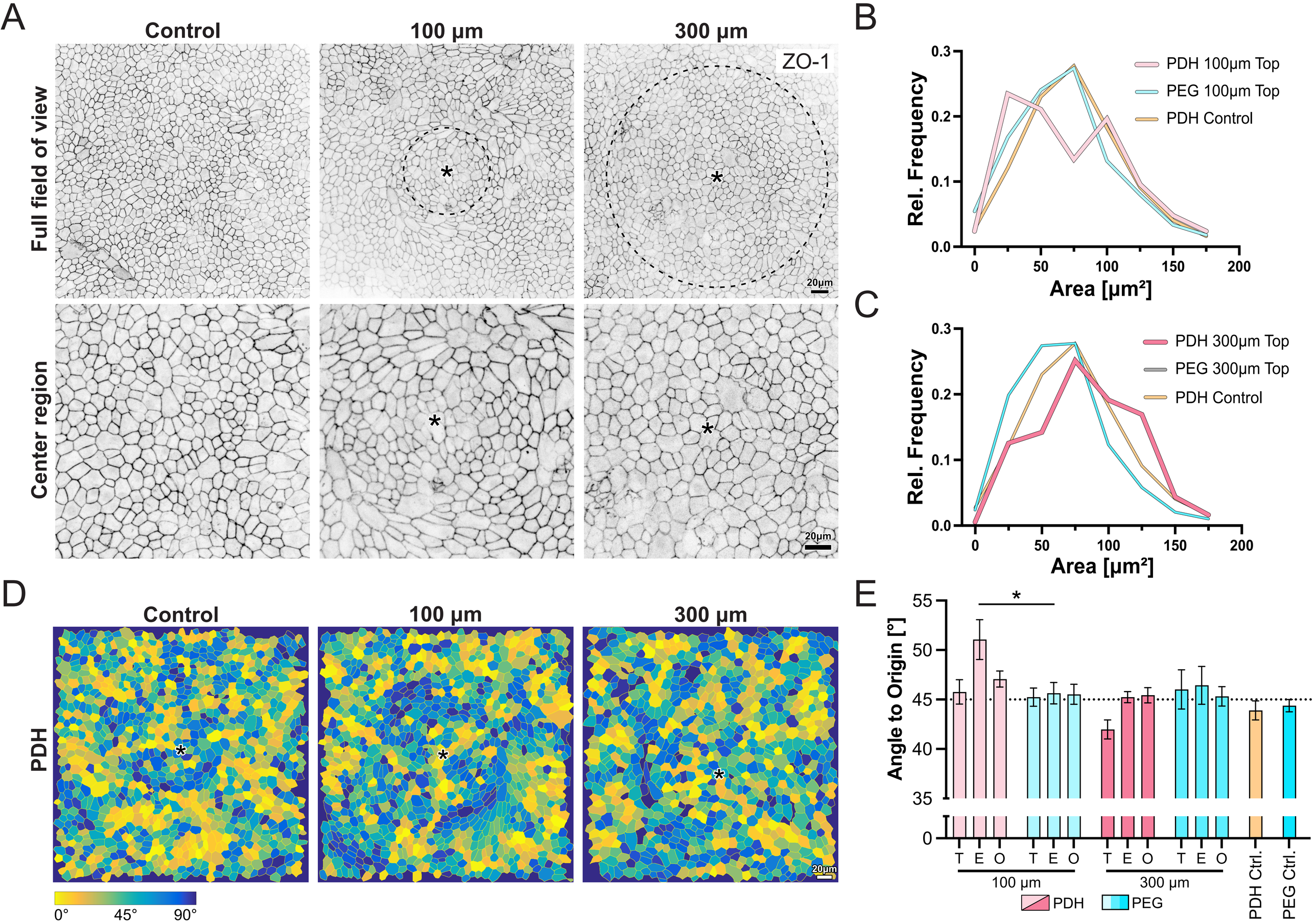
A
Control
100 µm
300 µm
Full field of view
Center region
ZO-1
20µm
B
PDH 100µm Top
PEG 100µm Top
PDH Control
Rel. Frequency
Area [µm²]
C
PDH 300µm Top
PEG 300µm Top
PDH Control
Rel. Frequency
Area [µm²]
D
Control
100 µm
300 µm
PDH
0°
45°
90°
E
Angle to Origin [°]
T E O T E O T E O T E O
100 µm
300 µm
PDH
PEG
PDH Ctrl.
PEG Ctrl.